

Understanding Cooperative Protein Adsorption Events at the Microscopic Scale: A Comparison between Experimental Data and Monte Carlo Simulations

Michael Rabe, Dorinel Verdes, and Stefan Seeger*

Institute of Physical Chemistry, University of Zurich, Winterthurerstrasse 190, 8057 Zurich, Switzerland

Received: October 7, 2009; Revised Manuscript Received: January 20, 2010

Cooperative effects play a vital role in protein adsorption events on biological interfaces. Despite a number of studies in this field molecular adsorption mechanisms that include cooperativity are still under debate. In this work we use a Monte Carlo-type simulation to explore the microscopic details behind cooperative protein adsorption. The simulation was designed to implement our previously proposed mechanism through which proteins are not necessarily rejected if they approach the surface to an occupied region. Instead, we suggest that proteins can be tracked laterally for a certain distance due to the influence of preadsorbed proteins in order to reach the nearest available binding site. The simulation results were compared with experimental data obtained by using the supercritical angle fluorescence (SAF) microscopy technique. It was found that the tracking distance may be up to 2.5 times the protein's diameter depending on the investigated system. The general validity of this tracking mechanism is supported by a number of linear or upward concave adsorption kinetics reported in the literature which are consistent with our simulation results. Furthermore, the self-organization of proteins adsorbing under cooperative conditions on the surface is shown to necessarily cause density inhomogeneities in the surface distribution of proteins which is also in agreement with experimental observations.

Introduction

In a number of experimental studies, cooperative effects have been found to play a major role in protein adsorption events.^{1–4} Unraveling the molecular details behind these effects is of great importance to understand the processes that regulate the activity and function of biological interfaces.^{5–7} Despite a large number of studies in this field, a unique opinion describing protein adsorption mechanisms including cooperativity is still lacking because most concepts concentrate on specific experimental observations, such as the formation of two-dimensional surface aggregates,^{2,8,9} sigmoidal adsorption isotherms,⁷ or characteristic adsorption kinetics.^{10–12} A more general point of view on cooperativity during protein adsorption includes all lateral interactions between adsorbed proteins. It has been reported that proteins in a crowded environment can have increased tendencies to undergo orientational or conformational reorientations^{11–13} or to preferably desorb, induced by the surrounding repulsive conditions.^{14,15} A clear sign for the presence of a cooperative adsorption process is the enhancement of protein adsorption due to other preadsorbed proteins, leading to partially constant or even increasing adsorption rates.^{1,3,4} In a recent study on cooperative adsorption, we attributed this phenomenon to an adsorption mechanism through which a protein can be guided or tracked to the nearest available binding site mediated by the complex electrostatic field of the charges contained in preadsorbed proteins and in the upper layer of the surface.¹⁶ This mechanism implies that prior to adsorption, a protein can move laterally for a certain distance when it approaches an occupied surface area. Using a special surface-sensitive microscopy technique based on the detection of supercritical angle fluorescence (SAF),¹⁷ we could relate two macroscopic observations with cooperative effects; namely, linear or even upward concave

adsorption kinetics and a patchy protein surface distribution composed of strongly and loosely populated regions. However, microscopic details, such as the length of the system-dependent tracking distance (r_{coop}) or the molecular assembly of proteins, were not amenable from the pure experiment.

An increasingly important access to molecular-scale studies of protein adsorption events has been opened by computational approaches. Molecular dynamics (MD) simulations, for instance, were applied to determine preferred orientations of adsorbed proteins and subsequent conformational reorientations. Unfortunately, these calculations are computationally too expensive for the study of cooperative effects between several proteins because details on the atomic level are considered. At the present, MD simulations are limited to small systems with one or two proteins and to time scales of a few nanoseconds.^{18–21} A promising step forward to larger systems is simulations based on coarse-grained models in which structural information is maintained in a strongly simplified manner.²² Although the simulated systems are still too small to investigate the effects of larger protein ensembles, important information, such as surface density, preferred orientations, or the effect of pH and ionic strength, is obtainable from this approach.^{23,24} With the lowest degree of structural information and, hence, the most simplified method, Metropolis Monte Carlo (MC) simulations are the only practicable solution to exploring large ensembles of adsorbed proteins on reasonable time scales.^{25,26} To evaluate the Metropolis condition, the potential energy has to be calculated after each MC step using appropriate pair-potential models. However, most models are based on crude approximations, such as a uniform, coverage-independent protein–surface potential that is essentially inappropriate for studying cooperative effects upon protein adsorption. An exact description of the potential energy near the surface would be a nontrivial, high-dimensional function considering the short- and long-range interactions between the adsorbing protein and all preadsorbed

* Corresponding author. Phone: +41-(0)44-6354451. Fax: +41-(0)44-6356813. E-mail: sseeger@pci.uzh.ch.

proteins plus the surface, at least in a local environment. This problem can be circumvented by replacing values resulting from approximate models with empirical parameters.^{27–30}

In this work, we investigate the microscopic events behind cooperative protein adsorption by means of a Monte Carlo-type simulation of an ensemble of thousands of adsorbing proteins. Using experimentally obtained rate constants as input parameters, we are able to correlate macroscopic observations, such as the characteristic adsorption kinetics, with the microscopic tracking distance (r_{coop}). In addition, the performed simulations let us understand why cooperative adsorption leads to inhomogeneous protein density distributions, which was also observed experimentally.¹⁶

Materials and Methods

Adsorption Model and Simulation. To achieve an accurate description of the experimentally obtained adsorption kinetics, we proposed two independent adsorption pathways for the binding of proteins to the surface. First, there is a noncooperative adsorption pathway (pathway 1) that takes place on empty surface regions without the influence of other preadsorbed proteins. According to its mathematical format, this pathway is equivalent to the classical Langmuir-type adsorption. It is important to note that the Langmuir theory is a crude approximation for particle adsorption on defined binding sites, which is certainly inappropriate for describing protein adsorption mechanisms.³¹ However, in this work, the error resulting from this approximation is generally small such that more accurate (and more complex) expressions are omitted, except for the case of pure noncooperative adsorption. The simple format allows for an analytical curve fit of experimental data without numerical integration. The second pathway (pathway 2) describes the cooperative adsorption through a guiding or tracking of a protein to the nearest available binding site if it approaches an already occupied surface region. The following mean field rate equations represent the macroscopic description of this model, assuming irreversible adsorption.¹⁶

$$\frac{d\theta_1}{dt} = k_1^{\text{on}} c \left(1 - \frac{\theta}{\theta_{\text{max}}}\right) \quad (1)$$

$$\frac{d\theta_2}{dt} = \begin{cases} k_2^{\text{on}} c \frac{\theta}{\theta_{\text{max}}}, & \frac{\theta}{\theta_{\text{max}}} \leq \alpha \\ k_2^{\text{on}} c \frac{\theta}{\theta_{\text{max}}} \frac{1}{1 - \alpha} \left(1 - \frac{\theta}{\theta_{\text{max}}}\right), & \frac{\theta}{\theta_{\text{max}}} > \alpha \end{cases} \quad (2)$$

In these equations, θ_1 and θ_2 denote the fraction of surface proteins adsorbed via the noncooperative (pathway 1) or the cooperative adsorption pathway (pathway 2), θ denotes the total surface coverage, and θ_{max} is the maximum coverage. k_1^{on} and k_2^{on} are the adsorption rate constants for the corresponding pathways, and c is the bulk protein concentration.

As discussed in detail in our previous work,¹⁶ the functional format of those equations predominantly results from the experimental observation that adsorption rates can be constant or even increase with growing protein density on the surface.^{1,10–12} For this reason, the factor $\theta/\theta_{\text{max}}$ needs to be included into the cooperative adsorption pathway (eq 2) to compensate for the noncooperative adsorption pathway (eq 1). Further, the cooperative adsorption pathway is modeled as a piecewise function to account for the fact that the slope of the adsorption kinetics abruptly decreases toward zero at a certain coverage level. At

low coverage levels, the rate-decreasing effect due to the continuous adsorption of proteins that occupy more and more binding sites is not observable. Such a counterintuitive behavior is generally explained by an electrostatic self-organization.^{1,10,12} This regime is represented by the upper part of eq 2, whereas the lower part of eq 2 refers to the stage in which the surface is strongly populated. Here, the limited number of available binding sites dominates the adsorption rate.

The point at which the observable adsorption rate changes between these two regimes is defined by the parameter α . Practically, α refers to the critical coverage level at which the adsorption rate decreases abruptly, resulting in a kink in the rate-coverage plots. The factor $(1 - \alpha)^{-1}$ has to be included in the lower part of eq 2 to avoid a mathematical point of discontinuity at $\theta = \alpha\theta_{\text{max}}$. To this end, the proposed rate equations represent a simple, though efficient, mean field formalism.

The exact environment of each adsorbed protein is not considered to avoid huge numbers of rate equations.⁹ All included parameters are accessible by a fit of the model to experimental data. The maximum coverage level, θ_{max} , corresponds to the final coverage level obtained after extended adsorption times (e.g., 2–4 h). The values of the rate constants k_1^{on} and k_2^{on} and of the parameter α follow directly from the curve shape of the adsorption kinetics, preferably presented as a rate-coverage plot (see ref 16 for a comprehensive analysis of experimental data).

A major limit of presenting the cooperative adsorption mechanism through rate equations (eqs 1 and 2) consists of the meaning of the parameter α . Because it is connected with the coverage level at which the lateral tracking of adsorbing proteins to an available binding site in the vicinity breaks down, α can be considered as an abstract measure for the maximum allowed lateral tracking distance, r_{coop} . The correlation between this macroscopically measurable parameter α and the real tracking distance, r_{coop} , can be obtained only through the microscopic MC simulation in which the proposed mechanism is implemented without abstraction.

This simulation was performed on a grid of 3250×3250 surface sites on which simulated proteins were sequentially adsorbed on random positions under periodic boundary conditions. The grid size was chosen to model a sufficiently large surface area corresponding to $6.5 \mu\text{m} \times 6.5 \mu\text{m}$ that accommodates around 10 million surface sites of $2 \text{ nm} \times 2 \text{ nm}$. The adsorbing proteins are chosen to exhibit a circular-like shape with a diameter equivalent to the length of seven surface sites, that is, 14 nm. Although this size was chosen to match the longest axis of the protein BSA,³² which was used predominantly in our experimental study, it is also well in the range of a number of common globular proteins. We emphasize that the protein radius used in this simulation refers to its effective interaction radius, which strongly depends on the protein's net charge and the surrounding pH.³³ The following algorithm was applied during the simulation:

1. A virtual protein is generated on the grid centered at a random position; if it does not overlap with any other preadsorbed protein, the step is accepted with the probability p_1 , which is proportional to the noncooperative adsorption rate constant ($p_1 \propto k_1^{\text{on}}$), and the next virtual protein is generated; the number of adsorption trials is incremented by 1.

2. If the protein does overlap with any preadsorbed protein, the nearest empty surface site on which the protein can adsorb without any overlap is evaluated; the adsorption on the new position is accepted with the probability p_2 ($p_2 \propto k_2^{\text{on}}$), provided

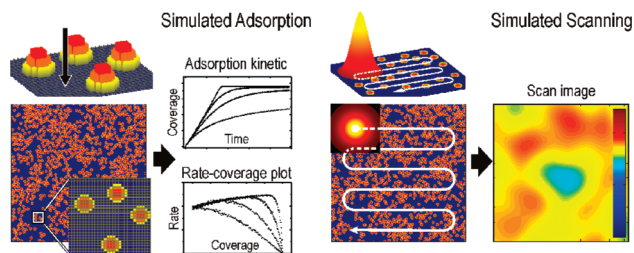


Figure 1. Overview of the Monte Carlo simulation. Adsorption kinetics (left) and scan images (right) are simulated and compared with experimental data.

the distance between the initial site and the new site is smaller or equal to the chosen cooperative radius r_{coop} ; otherwise, the protein is rejected. The next virtual protein is generated, and the number of adsorption trials is incremented by 1.

As schematically illustrated in Figure 1, the simulation gives access to the adsorption kinetics and to scan images, both of which can be directly compared to experimental data. The kinetics and the corresponding rate-coverage plots are simply obtained by counting all proteins on the $6.5 \mu\text{m} \times 6.5 \mu\text{m}$ surface in intervals of 250 adsorption trials or after ~ 6 trials on a $1.0 \mu\text{m} \times 1.0 \mu\text{m}$ surface, respectively. To determine the maximum coverage (θ_{max}) of each individual set of parameters, an extended simulation up to 1 million adsorption trials was performed to ensure that the system is in saturation. To obtain scan images during the simulation, a discrete convolution of the protein-covered surface with the point spread function of the experimental setup is performed in intervals of 10 000 adsorption trials:

$$s(x, y) = l(x, y) * f(x, y) = \sum_{\tau_y} \sum_{\tau_x} l(x - \tau_x, y - \tau_y) f(\tau_x, \tau_y) \quad (3)$$

where $s(x, y)$ is the function representing the intensity of the scan image, $l(x, y)$ refers to the point spread function, and $f(x, y)$ is the object function, that is, the protein-covered surface. The point spread function is modeled by a Gaussian function covering 1000×1000 surface sites, that is, $2.0 \mu\text{m} \times 2.0 \mu\text{m}$, with a width of $2\sigma = 0.5 \mu\text{m}$, which is in accordance with the instrumental response profile of the SAF microscope,¹⁷

$$l(x, y) = N e^{-(x^2+y^2)/2\sigma^2} \quad (4)$$

where N is the normalization factor that is chosen such that the scan image of a saturated surface scales to an average intensity of 100%. During the convolution process, the movement of the point spread function $l(x, y)$ is restricted such that it never exceeds the area of the object function to exclude errors at the boundaries of the simulated area. As a result, the simulated scan image exhibits a size of 2250×2250 surface sites, that is, $4.5 \mu\text{m} \times 4.5 \mu\text{m}$. The total surface size of $6.5 \mu\text{m} \times 6.5 \mu\text{m}$ turned out to be large enough to ensure that variations of the final coverage levels are well below 0.1%.

Preparation of Buffers and the Protein Solution. The adsorption of the protein bovine serum albumin (BSA) on glass coverslips (Menzel, Germany) is used as experimental comparison for the simulation results presented herein. In agreement with our previous results, cooperative adsorption conditions were realized by using citrate buffer (50 mM) at pH 3 and a protein bulk concentration of 8 nM. Noncooperative conditions were

realized by using citrate buffer (50 mM) at pH 4.85, corresponding to the pI of BSA and a protein bulk concentration of 64 nM. Citrate buffer (50 mM) was prepared by dissolving 10.5 g of citric acid (Riedel de Haen, Switzerland) in 1.0 L of water and subsequent titration with NaOH (5 N) (Fluka, Switzerland) to obtain a pH of 3. Carbonate buffer (50 mM) was prepared by dissolving 4.2 g of NaHCO_3 (Fluka, Switzerland) in 1.0 L of water and adjusting the pH to 9.3 with HCl (1 N) (Acros, Switzerland). The protein bovine serum albumin (BSA, A-4378, >97% protein) was obtained from Sigma (Switzerland) and used as received. DY-647-monofunctional *N*-hydroxysuccinimide ester dye (Dyomics, Germany) was used as the fluorescent label. The coupling of the dye to the protein was conducted by adding 1.0 mL of protein dissolved in carbonate buffer, pH 9.3 (20 mg/mL, BSA) to 0.2 mg of lyophilized DY-647-NHS. The mixture was kept at room temperature for about one hour under slight agitation, leading to a dye-to-protein ratio of 1.05, as was determined by UV/vis spectroscopy. Unreacted dye was separated from labeled proteins via size exclusion chromatography using a Superdex 200 10/300 GL column (Amersham, U.K.). All solutions were stored at 4 °C in the dark. Buffer solutions were filtered using a 0.22 μm pore size membrane filter (Millipore, Switzerland) prior to use.

Surface Imaging and Analysis. Experimental surface scan images were obtained using the surface-sensitive SAF microscope, which has been proven to be a reliable tool for several protein adsorption studies.^{11,34–36} The technique is based on the selective and highly sensitive detection of fluorophores near the dielectric interface, whereas the fluorescence coming from the bulk solution is efficiently rejected.^{37,38} A scanning microscope table moves the measuring cell over the objective of the microscope, and hence, up to $75 \mu\text{m} \times 75 \mu\text{m}$ areas can be imaged with diffraction-limited resolution (see refs 17 and 39 for a detailed description of the optical setup). The protein density distribution was followed by repeatedly recording the intensity image of one surface area ($75 \mu\text{m} \times 75 \mu\text{m}$) under a constant supply of protein solution through a flow cell. All experimental images were subjected to a nearest-neighbor averaging prior to plotting and further analysis. To perform the statistical analysis of the surface inhomogeneities, 30 subsections ($4.5 \mu\text{m} \times 4.5 \mu\text{m}$) of the experimental scan image were chosen in which the difference between maximum and minimum intensity was determined. These values were combined to calculate the mean maximum difference and its standard error. To obtain analogous data from the MC simulation, 100 individual simulations on a small area ($6.5 \mu\text{m} \times 6.5 \mu\text{m}$) were run. After convolution using the artificial point spread function ($2 \mu\text{m} \times 2 \mu\text{m}$), a simulated scan image ($4.5 \mu\text{m} \times 4.5 \mu\text{m}$) was obtained from which the maximum and minimum intensities were extracted.

Results and Discussion

The Length of the Cooperative Radius. To quantify the correlation between the length of the cooperative radius r_{coop} and the parameter α , the influence of varying r_{coop} on the resulting adsorption kinetics has to be explored. Therefore, we ran 18 simulations with values of r_{coop} ranging between 0 and 7.5 in units of the protein's diameter. The adsorption probability ratio between cooperatively and noncooperatively adsorbing proteins was set to $p_2/p_1 = 1.3$, which corresponds exactly to the observed ratio between $k_2^{\text{on}}/k_1^{\text{on}}$ in the case of BSA adsorption on glass at pH 3.¹⁶ Mechanistically, this ratio implies that bulk proteins approaching the surface at an occupied binding site

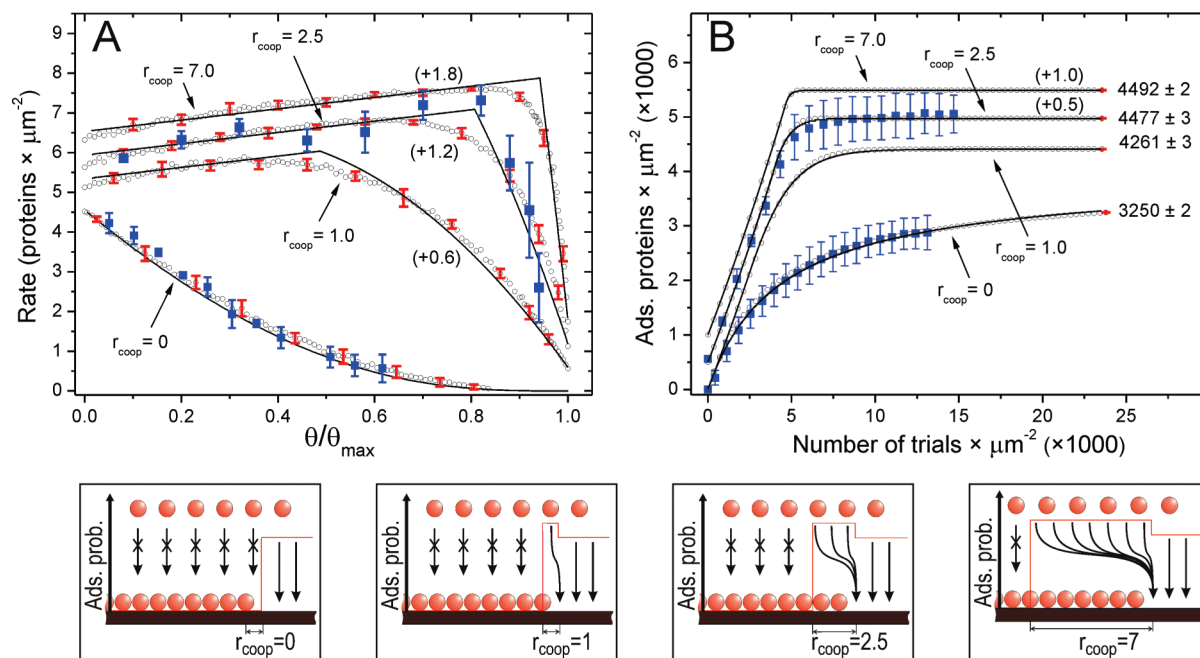


Figure 2. Simulated rate-coverage plots (A) and the corresponding adsorption kinetics (B) for varying r_{coop} . From bottom to top: 0, 1.0, 2.5, and 7.0. The simulated data points (black circles) were fitted using the macroscopic description of the model (solid lines). For the sake of clarity, some of the curves were shifted upward. Red error bars indicate the variation among 10 repeated simulations at different stages during the adsorption. Experimental data (blue squares) obtained from BSA adsorption at pH 4.85 (bottom) and pH 3 (top) were added to the curves corresponding to $r_{\text{coop}} = 0$ and $r_{\text{coop}} = 2.5$. The following time calibration was applied: pH 4.85 ($c = 64$ nM), one adsorption trial corresponds to 1.7 s; pH 3 ($c = 8$ nM), one adsorption trial corresponds to 0.8 s. The schematic illustrations underneath present the tracking mechanism at different values of r_{coop} . Proteins approaching the surface at an occupied region adsorb with increased probability, provided they are within the cooperative radius. Black arrows indicate the allowed (solid arrow) and forbidden (broken arrow) adsorption pathways of proteins near the interface. The red curve schematically shows the adsorption probability above a certain position.

are more strongly tracked toward the surface than proteins approaching an unoccupied surface region. This can be understood considering that on negatively charged surfaces, proteins adopt an orientation in which the majority of their positively charged regions are directed toward the surface and the majority of their negatively charged regions are directed toward the bulk solution. Such a constellation enhances the attraction of further bulk proteins.^{32,40}

As stated before, the longer the tracking distance, the higher the value of α . Thus, a curve fit of the rate equations (eqs 1 and 2) to the simulated kinetic data yields a specific value of α for every chosen r_{coop} . In this way, the link between the macroscopic and the microscopic perspective is made. Examples of the simulation results for differing cooperative radii are shown in Figure 2 plotted as rate-coverage plots (A) and adsorption kinetics (B). The fit of the model is added in all plots as a thin, solid line and shows nicely the smooth transition between increasing and decreasing adsorption rates in the simulation data (circles). Thus, the sharp kink in the rate-coverage plots can be eliminated because the simulation works without the abstract parameter α and without the piecewise function defined by eq 2. Only the maximum tracking distance, r_{coop} , and the two rate constants k_1^{on} and k_2^{on} (herein the ratio $p_2/p_1 = k_2^{\text{on}}/k_1^{\text{on}}$ is used) determines the shape of the adsorption kinetics. Naturally, the macroscopic approach represented by the rate equations 1 and 2 is computationally much less demanding and, therefore, still provides an efficient alternative to describe the observed adsorption kinetics. In fact, the time-integrated adsorption kinetics resulting from the two methods, macroscopic and microscopic, can even hardly be distinguished from one another (compare Figure 2 B, solid lines and circles).

In Figure 3, simulation results obtained at a fixed cooperative radius ($r_{\text{coop}} = 1.0$) and varying ratios of p_2/p_1 are presented.

Clearly, this ratio determines the initial slope of the adsorption rate plotted as a function of the surface coverage (see Figure 3A). It is obvious that the fit of the rate equations presented as solid lines becomes weaker the higher the ratio p_2/p_1 that is chosen. Considering the approximations inherent to the rate equations, this is an expected outcome. Comparing the time-integrated adsorption kinetics shown in Figures 2B and 3B, it is also nicely visible that differences resulting from various r_{coop} or p_2/p_1 ratios are extremely subtle. To this end, rate-coverage plots are crucial to properly investigate the adsorption behaviors.

Plotting the parameter α resulting from the curve fits as a function of r_{coop} yields the aspired connection between an experimentally amenable information and its microscopic interpretation (Figure 4). One consequence of this plot is that a value of $\alpha = 0.8$, which is around the experimental value found for BSA adsorption on glass at pH 3, corresponds to a cooperative radius of about $r_{\text{coop}} = 2.5$, that is, 35 nm. That means proteins that approach the surface at an occupied position can be tracked up to a distance of 2.5 times their own diameter toward an available surface site (see Figure 2, schemes). To highlight the agreement between simulated adsorption kinetics and experimental data, the recorded kinetics corresponding to BSA adsorption in citrate buffer (50 mM) at pH 3 were overlaid with the plots in Figure 2 referring to $r_{\text{coop}} = 2.5$ (blue squares). Typical experimental values for the parameter α in the case of cooperative adsorption are between 0.31 and 0.84.¹⁶ Referring to Figure 4, the underlying cooperative radii thus range from 0.75 up to 3.0 (10.5–42 nm). Because no larger r_{coop} was found experimentally, the upper curve in Figure 2A and B ($r_{\text{coop}} = 7.0$) is a pure theoretical one which most probably has no realistic meaning.

To better highlight the effect of the cooperative adsorption pathway on the shape of the adsorption kinetics, a reference

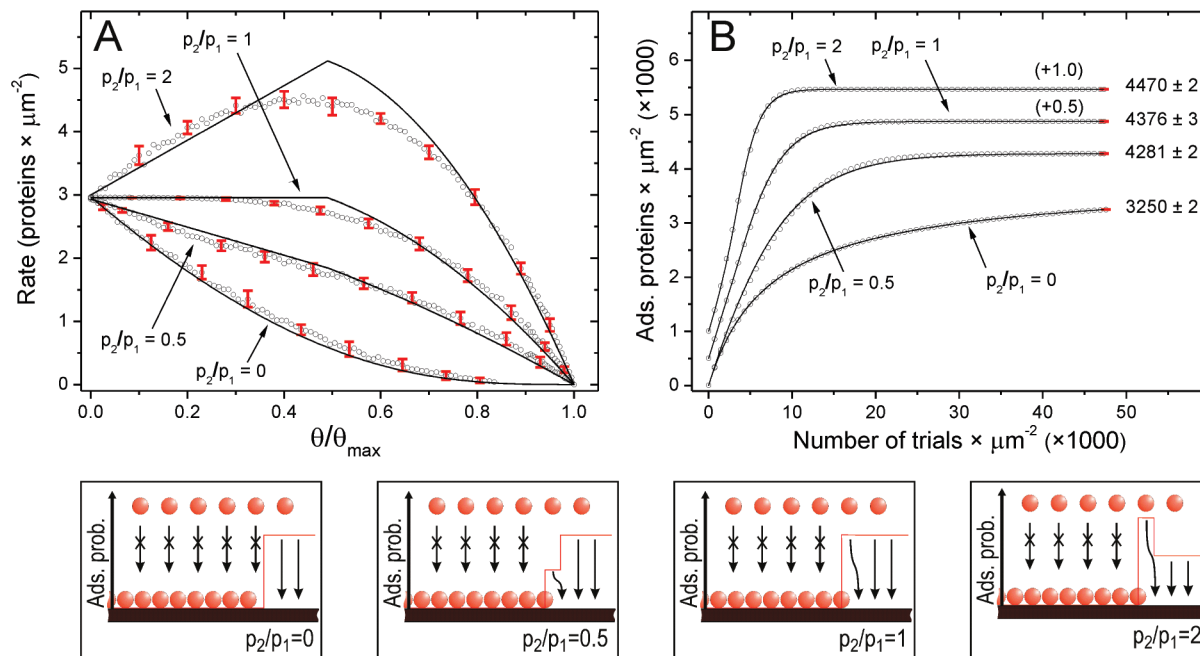


Figure 3. Simulated rate-coverage plots (A) and corresponding adsorption kinetics (B) for varying p_2/p_1 ratios. From bottom to top: 0, 0.5, 1.0, and 2.0. The noncooperative adsorption probability, p_1 , was kept fixed at 0.5 for all simulations. The simulated data points (black circles) were fitted using the macroscopic description of the model (solid lines). Red error bars indicate the variation among 10 repeated simulations at different stages during the adsorption. The schematic illustrations underneath present the tracking mechanism at different values of p_2/p_1 .

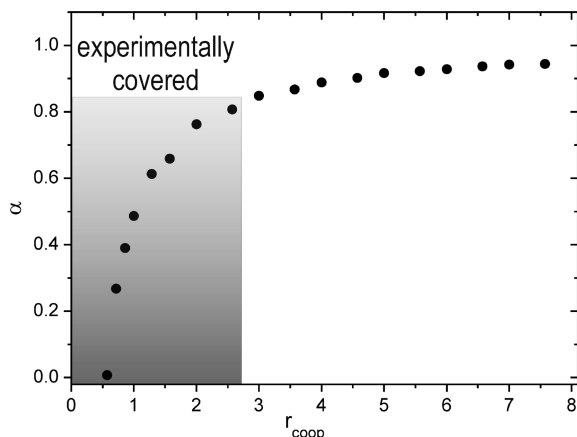


Figure 4. Correlation between the macroscopic parameter α and the microscopic value of r_{coop} .

simulation using $r_{\text{coop}} = 0$ was run (lower curves in Figures 2A, B and 3A, B). In this case, the adsorption rate steadily declines with the increasing coverage because the available surface area decreases. The characteristic convex shape of the rate-coverage plot is a result of size-exclusion effects that are necessarily involved in the simulated adsorption process, since each protein occupies more than only one surface site (namely, 37). Using the formalism developed in the framework of the random sequential adsorption (RSA) theory, the simulated adsorption kinetics under noncooperative conditions can be accurately described by (lowest solid lines in Figure 2 A, B and Figure 3 A, B)⁴¹

$$\frac{d\theta}{dt} = k_1^{\text{on}} c \frac{\left(1 - \frac{\theta}{\theta_j}\right)^3}{1 - 0.812\left(\frac{\theta}{\theta_j}\right) + 0.2336\left(\frac{\theta}{\theta_j}\right)^2 + 0.0845\left(\frac{\theta}{\theta_j}\right)^3} \quad (5)$$

Experimentally, a pure noncooperative scenario was found in the case of BSA adsorption on glass at pH = pI. The corresponding data are added to the simulation results of $r_{\text{coop}} = 0$ in Figure 2 (blue squares).

Self-Organization of Adsorbed Proteins. As stated earlier, protein layers that form on surfaces under cooperative adsorption conditions show a certain degree of inhomogeneity with respect to their density distribution. To explore this characteristic self-organization of proteins on the microscopic scale, simulated scanning was performed at different coverage levels in the course of simulated adsorption. The parameters for this simulation were fixed to $r_{\text{coop}} = 2.5$ and $p_2/p_1 = 1.3$ because these values were found from a data analysis of BSA adsorption at pH 3. In the following, this experimental system is used as a comparison for our simulation results.

Figure 5 summarizes the simulated arrangement of surface adsorbed proteins at different coverage levels (middle column, complete view; left column, magnified view). The convoluted images displaying the simulated scan images are shown in the right column of Figure 5. Since periodic boundary conditions were used and since the scanned area never exceeds the edges of the protein-containing matrix, finite size effects can be excluded. In the center of these images, one can notice a local intensity minimum; thus, a region of low protein density. This local minimum is present in practically all scan images ranging from a total coverage of $\sim 25\%$ in the beginning up to $\sim 80\%$ after 180 000 adsorption trials on the $6.5 \mu\text{m} \times 6.5 \mu\text{m}$ surface. The profile plots (inset in Figure 5) reveal that the intensity difference between the low density region in the center and the high density region in the circumference scales to $\sim 8\%$ of the saturation coverage. To work out the major characteristics of cooperative protein adsorption, the results shown in Figure 5 are compared with a reference simulation of a pure, noncooperative adsorption ($r_{\text{coop}} = 0$) presented in Figure 6 (see the Supporting Information for two other reference simulations conducted at $r_{\text{coop}} = 1.0$ and $r_{\text{coop}} = 5.0$).

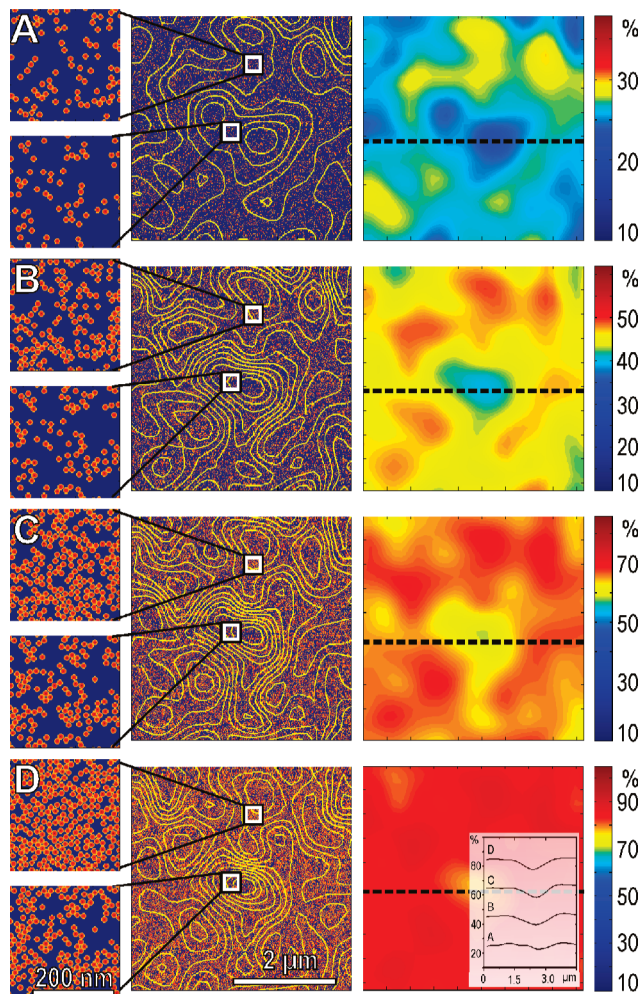


Figure 5. Simulated scanning during cooperative adsorption at $r_{\text{coop}} = 2.5$ and $p_2/p_1 = 1.3$. The protein distribution on the surface (middle and left column) and the corresponding scan images (right column) are presented. Inset: Profile plots along the dashed lines. Sampling was performed after 60 (A), 100 (B), 140 (C), and 180 (D) $\times 10^3$ adsorption trials on the $6.5 \mu\text{m} \times 6.5 \mu\text{m}$ surface. Contour lines show the regions of constant protein density.

As can be clearly seen in the simulated scan images, protein density variations in the noncooperative case are less pronounced because they scale only to a maximum of $\sim 4\%$ of the saturation coverage (see profile plots in the inset of Figure 6). Moreover, the distribution of regions of higher and lower protein density at an early point in time is clearly uncorrelated with their distribution at a later point in time. In contrast to the behavior under cooperative conditions (Figure 5), the contour lines in the middle column of Figure 6 indicate randomly changing positions of regions of higher and lower protein density. This observation is the expected result of a simple noncooperative adsorption behavior: if there are differences in the protein density on the surface resulting from random processes, they are balanced out during the course of further adsorption. Thus, the simulation reveals that the cooperative adsorption process is directly linked to inhomogeneities in the surface distribution of adsorbed proteins. During their continuous adsorption, proteins arrange spontaneously in such a way that regions of higher occupancy and regions of lower occupancy are observed in the scan images. Examples for such protein arrangements are shown as magnified views on the left of Figure 5. By contrast, intensity inhomogeneities are also found during noncooperative adsorption, but to a significantly lower extent

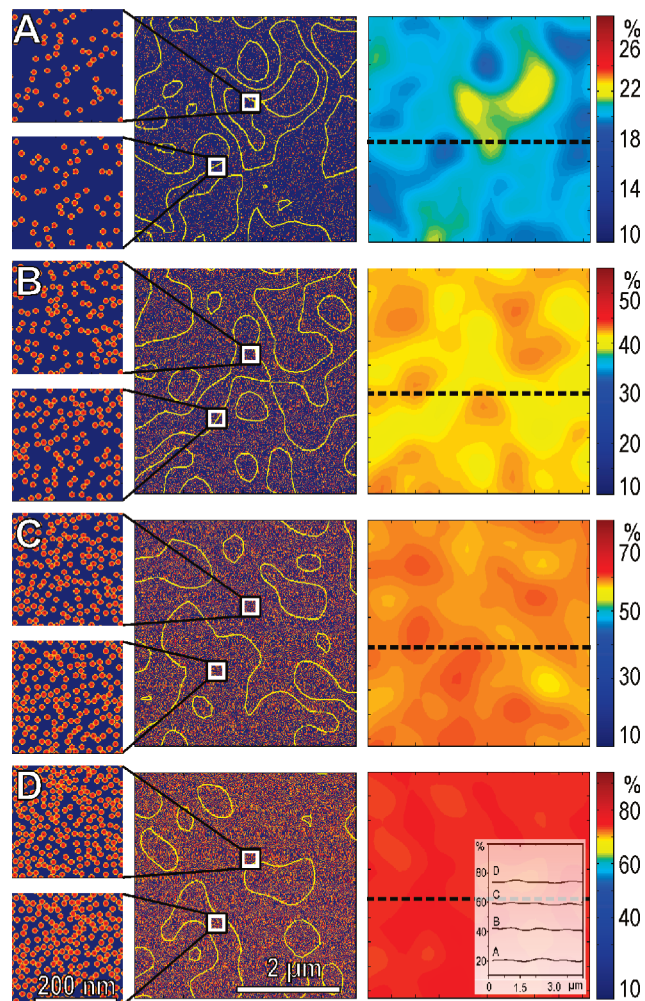


Figure 6. Simulated scanning during noncooperative adsorption at $r_{\text{coop}} = 0$. Scan images (right) and contour lines (middle) show changing distributions of high and low density regions. The protein distribution is more homogeneous at all times (left). Sampling was performed after 60 (A), 180 (B), 400 (C), and 1000 (D) $\times 10^3$ adsorption trials on the $6.5 \mu\text{m} \times 6.5 \mu\text{m}$ surface. Contour lines show the regions of constant protein density.

than in the case of cooperative adsorption. Accordingly, the protein arrangements (Figure 6, left) are of nearly uniform appearance.

The typical adsorption behaviors are also observed experimentally when the scan images of protein adsorption at different coverage levels are compared under cooperative and noncooperative conditions (Figure 7). Only cooperative adsorption (Figure 7, left column) leads to a surface distribution pattern that remains similar at increasing coverage. Noncooperative adsorption (Figure 7, right column), in contrast, causes randomly changing surface distribution patterns. Some areas in which the protein density is low in the beginning may even become regions of high density at a later point in time.

To highlight that the surface inhomogeneities are significantly more pronounced in the case of cooperative adsorption, as compared to noncooperative adsorption, a statistical evaluation of the intensity variations was performed. Therefore, 100 independent simulations for each case were run starting from an empty surface, and simulated scanning was performed with each simulation at distinct coverage levels. Naturally, the extent of the inhomogeneities in the protein surface densities is dependent on the cooperative radius r_{coop} and the ratio between

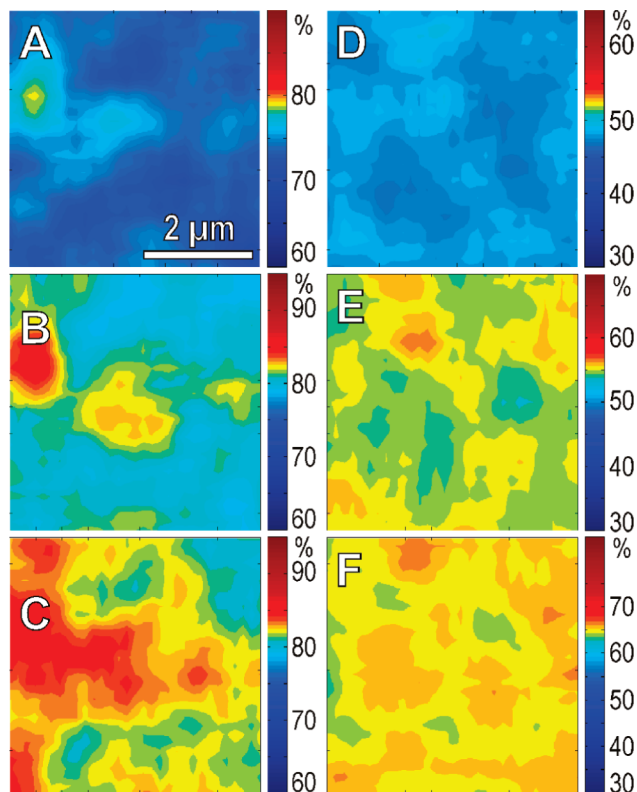


Figure 7. Experimentally obtained scan images during BSA adsorption using the SAF microscope. Proteins adsorbing under cooperative (left column) and noncooperative (right column) conditions are compared. Scan images were recorded after 100 (A), 125 (B), and 135 (C) min at a bulk concentration of 8 nM for the cooperative adsorption and after 40 (D), 50 (E), and 75 (F) min at 64 nM for the noncooperative adsorption.

cooperative and noncooperative adsorption probability p_2/p_1 . In Figure 8A, the mean differences between maximum and minimum intensities of the simulated scan images are plotted as a function of the surface coverage simulated for varying cooperative radii at a fixed p_2/p_1 ratio. The red curve in Figure 8A corresponds to $r_{\text{coop}} = 2.5$ and $p_2/p_1 = 1.3$, which are the experimentally found parameters for cooperative adsorption of BSA. The black curve in Figure 8A results from the simulation of pure noncooperative adsorption; that is, $r_{\text{coop}} = 0$. As expected, the intensity of protein density fluctuations decreases when lowering the cooperative radius. Figure 8B presents the protein density fluctuations resulting from varying p_2/p_1 ratios at a fixed cooperative radius of $r_{\text{coop}} = 1.0$. It shows clearly that the density inhomogeneities are stronger the higher the ratio p_2/p_1 that is chosen. When the simulated fluctuation curves of cooperative adsorption (red, blue, and green curves in Figure 8A, B) and noncooperative adsorption (black curves in Figure 8A, B) are compared, it turns out that intensity fluctuations of up to 4% of the saturation coverage appear in the beginning in both cases. However, during the noncooperative adsorption, variations are quickly balanced out when the surface coverage increases, whereas during the cooperative adsorption, the initial density fluctuations provoke the formation of even stronger intensity differences after continued adsorption. Only when the system comes closer to its saturation level are the density fluctuations naturally balanced out. As a consequence, the difference among the surface inhomogeneities becomes most obvious at coverage levels between 50% and 80%.

An analogous analysis was performed on the experimental results using 30 subsections of a large scan image that was

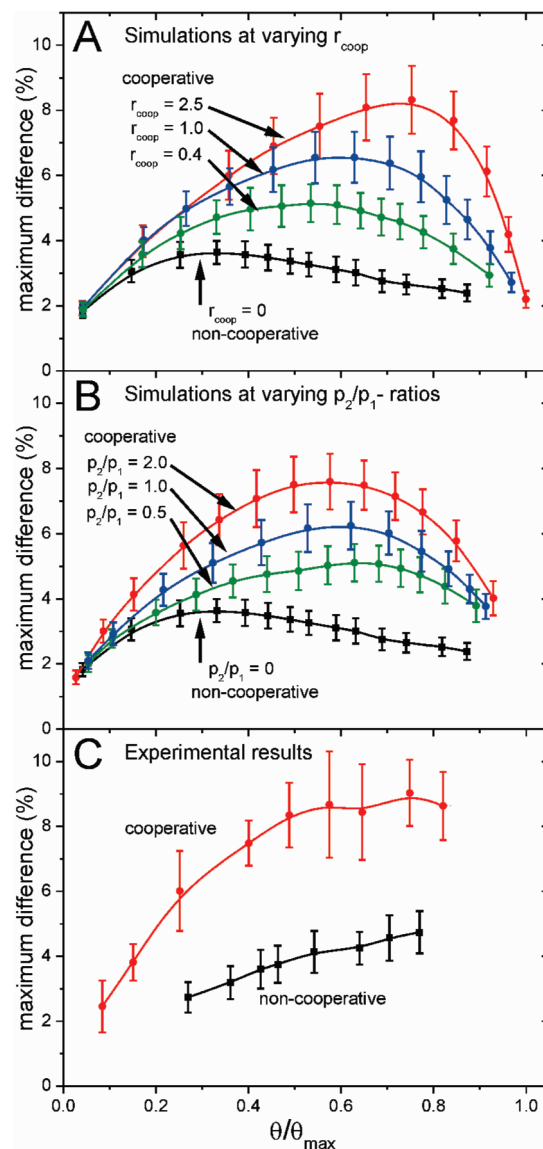


Figure 8. Statistical evaluation of density variations in the scan images at different adsorption stages. The average difference between intensity maximum and minimum of the scan images was plotted as a function of the surface coverage. (A) Simulation results for varying cooperative radii (2.5, red; 1.0, blue; 0.4, green; 0, black) at a fixed p_2/p_1 ratio of 1.3. (B) Simulation results for varying p_2/p_1 ratios (2.0, red; 1.0, blue; 0.5, green; 0, black) at a fixed cooperative radius of 1.0. (C) Experimental results for BSA adsorption at pH 3 (red) and pH 4.85 (black).

repeatedly scanned until protein adsorption reached the saturation level. The plots of the maximum intensity differences presented in Figure 8C suggest qualitative agreement between observed and simulated protein surface distributions. However, the most important conclusion from this analysis is that inhomogeneities resulting from cooperative adsorption are significantly stronger as compared to noncooperative adsorption, and this is true for the simulation as well as for the experiment. It is, of course, impossible to extract quantitative information about r_{coop} and the ratio p_2/p_1 from a comparison of the simulation results (Figure 8A and B) and the experimental results (Figure 8C). However, those parameters are already known from the kinetic analyses, and thus, the experimentally obtained scan images shown in Figure 7 are consistent with the proposed mechanism of cooperative adsorption. Because of the tracking or guiding behavior, proteins organize preferably in patches of

high protein density that naturally also leave behind some regions of low protein density. Such a self-organization is recognized as an inhomogeneous intensity image when the surface is scanned with the SAF microscope.

Conclusion

In the present study, we explore the microscopic events behind the cooperative adsorption of proteins to solid surfaces with the help of a Monte Carlo-type simulation. The implemented algorithm represents our proposed mechanism of cooperative adsorption whose key feature is that a protein approaching the surface in an occupied region is not necessarily rejected like in the classical Langmuir-type adsorption model. Instead, the protein is tracked to the nearest available binding site guided by the complex local electrostatic field arising from the preadsorbed charged proteins and the surface. From the simulation data, we extracted information with regard to the adsorption kinetics and to the self-organization of adsorbed proteins. The simulation settings and conditions are chosen such that a direct comparison with experimental results is possible. First, simulated adsorption kinetics are found to be in excellent agreement with experimental data and with the calculated kinetics using the proposed rate equations (eqs 1 and 2) (see Figure 2). Compared to this macroscopic approach, however, the simulation certainly represents a more realistic situation because it works without the abstract parameter α . Thus, the piecewise description of the adsorption rate as is implemented in eq 2 becomes superfluous, and the kink in the rate coverage plots can be avoided. In fact, the simulation reveals that there is, indeed, a sharp transition between the increasing and decreasing parts of the adsorption rate, but this appears clearly not in a steplike fashion. However, the accuracy of experimental data is insufficient for an unambiguous assignment of the transition behavior. We therefore consider the macroscopic approach as a straightforward and sufficiently accurate method to evaluate experimental adsorption kinetics. Since the present study provides a correlation between the parameter α and the tracking distance, r_{coop} , a microscopic interpretation of experimental data is now possible.

Apart from the adsorption kinetics, we also explored the self-organization behavior of proteins from a microscopic point of view. It was found that the random adsorption of proteins on a surface causes minute density fluctuations which, under cooperative conditions, evolve into persistent density differences after continued adsorption. The simulation reveals that cooperative adsorption causes the formation of patches of large numbers of proteins next to loosely covered surface regions. Macroscopically, this necessarily results in the observed scan images showing characteristic density inhomogeneities. To demonstrate that the discussed effects are tightly connected to cooperativity, reference simulations and experimental results obtained under noncooperative conditions were shown for comparison (Figures 5–8).

Because of the wide agreement between various macroscopic observations with the results of the simulation presented herein, we consider this study to highlight the validity of relating cooperative adsorption to the proposed tracking or guiding mechanism which has, to our knowledge, not been formulated in such a straightforward manner before.

Acknowledgment. The authors thank the Swiss National Science Foundation (SNSF) and the Forschungskredit of the University of Zurich for financial support.

Supporting Information Available: Reference simulations were performed using $r_{\text{coop}} = 1.0$ and $r_{\text{coop}} = 5.0$ at a p_2/p_1 ratio of 1.3. The simulated scan images and the protein distribution are shown in Figures S1 and S2. This material is available free of charge via the Internet at <http://pubs.acs.org>.

References and Notes

- (1) Ball, V.; Ramsden, J. *J. Phys. Chem. B* **1997**, *101*, 5465.
- (2) Herrig, A.; Janke, M.; Austermann, J.; Gerke, V.; Janshoff, A.; Steinem, C. *Biochemistry* **2006**, *45*, 13025.
- (3) Nygren, H.; Alaeddin, S.; Lundström, I.; Magnusson, K. E. *Biophys. Chem.* **1994**, *49*, 263.
- (4) Van der Veen, M.; Stuart, M. C.; Norde, W. *Colloids Surf., B* **2007**, *54*, 136.
- (5) Hinderliter, A.; Almeida, P. F. F.; Creutz, C. E.; Biltonen, R. L. *Biochemistry* **2001**, *40*, 4181.
- (6) Hinderliter, A.; Biltonen, R. L.; Almeida, P. F. F. *Biochemistry* **2004**, *43*, 7102.
- (7) Hinderliter, A.; May, S. *J. Phys.: Condens. Matter* **2006**, *18*, 1257.
- (8) Minton, A. P. *Biophys. Chem.* **2000**, *86*, 239.
- (9) Minton, A. P. *Biophys. J.* **2001**, *80*, 1641.
- (10) Ball, V.; Ramsden, J. *Colloids Surf., B* **2000**, *17*, 81.
- (11) Rabe, M.; Verdes, D.; Rankl, M.; Artus, G. R. J.; Seeger, S. *ChemPhysChem* **2007**, *8*, 862.
- (12) Vasina, E. N.; Dejardin, P. *Langmuir* **2004**, *20*, 8699.
- (13) Daly, S. M.; Przybycien, T. M.; Tilton, R. D. *Langmuir* **2003**, *19*, 3848.
- (14) Kurrat, R.; Ramsden, J. J.; Prenosil, J. E. *J. Chem. Soc., Faraday Trans.* **1994**, *90*, 587.
- (15) Tie, Y.; Calonder, C.; Van Tassel, P. R. *J. Colloid Interface Sci.* **2003**, *268*, 1.
- (16) Rabe, M.; Verdes, D.; Zimmermann, J.; Seeger, S. *J. Phys. Chem. B* **2008**, *112*, 13971.
- (17) Verdes, D.; Ruckstuhl, T.; Seeger, S. *J. Biomed. Opt.* **2007**, *12*, 034012.
- (18) Nonella, M.; Seeger, S. *ChemPhysChem* **2008**, *9*, 414.
- (19) Hagiwara, T.; Sakiyama, T.; Watanabe, H. *Langmuir* **2009**, *25*, 226.
- (20) Raffaini, G.; Ganazzoli, F. *Langmuir* **2004**, *20*, 3371.
- (21) Raffaini, G.; Ganazzoli, F. *J. Mater. Sci.: Mater. Med.* **2007**, *18*, 309.
- (22) Tozzini, V. *Curr. Opin. Struct. Biol.* **2005**, *15*, 144.
- (23) Carlsson, F.; Hyllner, E.; Arnebrant, T.; Malmsten, M.; Linse, P. *J. Phys. Chem. B* **2004**, *108*, 9871.
- (24) Skepö, M. *J. Chem. Phys.* **2008**, *129*, 185101.
- (25) Bellion, M.; Santen, L.; Mantz, H.; Hahl, H.; Quinn, A.; Nagel, A.; Gilow, C.; Weitenberg, C.; Schmitt, Y.; Jacobs, K. *J. Phys.: Condens. Matter* **2008**, *20*, 404226.
- (26) Quinn, A.; Mantz, H.; Jacobs, K.; Bellion, M.; Santen, L. *EPL* **2008**, *81*, 56003.
- (27) Mulheran, P. A.; Pellenc, D.; Bennett, R. A.; Green, R. J.; Sperrin, M. *Phys. Rev. Lett.* **2008**, *1*, 068102.
- (28) Pellenc, D.; Bennett, R. A.; Green, R. J.; Sperrin, M.; Mulheran, P. A. *Langmuir* **2008**, *24*, 9648.
- (29) Pellenc, D.; Gallet, O.; Berry, H. *Phys. Rev. E* **2005**, *72*, 051904.
- (30) Zhdanov, V. P.; Kasemo, B. *Proteins: Struct., Funct., Genet.* **2000**, *40*, 539.
- (31) Ramsden, J. J. Kinetics of protein adsorption. In *Biopolymers at Interfaces*; Malmsten, M., Ed.; Marcel Dekker, 1998; pp 321.
- (32) Su, T. J.; Lu, J. R.; Thomas, R. K.; Cui, Z. F.; Penfold, J. *J. Phys. Chem. B* **1998**, *102*, 8100.
- (33) Ravichandran, S.; Talbot, J. *Biophys. J.* **2000**, *78*, 110.
- (34) Rankl, M.; Ruckstuhl, T.; Rabe, M.; Artus, G. R. J.; Walser, A.; Seeger, S. *ChemPhysChem* **2006**, *7*, 837.
- (35) Rabe, M.; Verdes, D.; Seeger, S. *Soft Matter* **2009**, *5*, 1039.
- (36) Zimmermann, J.; Rabe, M.; Verdes, D.; Seeger, S. *Langmuir* **2008**, *24*, 1053.
- (37) Enderlein, J.; Ruckstuhl, T.; Seeger, S. *Appl. Opt.* **1999**, *38*, 724.
- (38) Ruckstuhl, T.; Enderlein, J.; Jung, S.; Seeger, S. *Anal. Chem.* **2000**, *72*, 2117.
- (39) Ruckstuhl, T.; Verdes, D. *Opt. Express* **2004**, *12*, 4246.
- (40) Bremer, M. G. E. G.; Duval, J.; Norde, W.; Lyklema, J. *Colloids Surf., A* **2004**, *250*, 29.
- (41) Schaaf, P.; Talbot, J. *J. Chem. Phys.* **1989**, *91*, 4401.